Journal of Materials Chemistry A

Accepted Manuscript

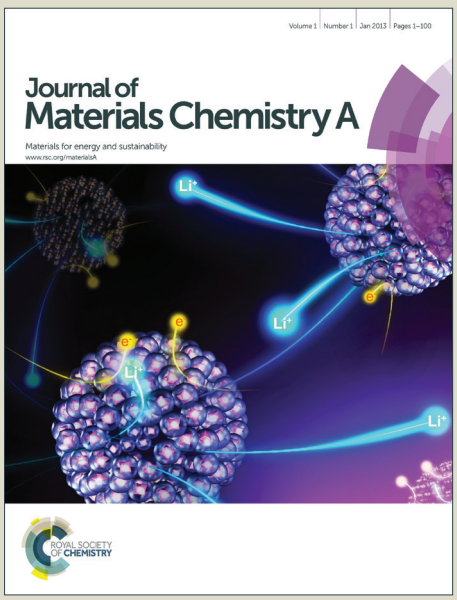

ROYAL SOCIETY OF CHEMISTRY

www.rsc.org/materialsA

ARTICLE TYPE www.rsc.org/xxxxxx | XXXXXXXX

Design and Synthesis of Functional Ionic Liquids Based on Pyrrolidinium Cations Bearing Alkyl Nitrile Moieties

Shan Cong,[a] Yun Wang,[a] Qinghua Yi,[a] Jie Zhao,*[a] Yinghui Sun,[a] Mingrong Shen[b] and Guifu Zou*[a]

Received (in XXX, XXX) Xth XXXXXXXXX 20XX, Accepted Xth XXXXXXXXX 20XX
DOI: 10.1039/b000000x

A series of functional ionic liquids based on pyrrolidinium cations bearing alkyl nitrile moieties have been designed, synthesized and charactered with high purity and yield. The influence of the anion structure and methylene chain length of alkyl nitrile moieties on the thermal properties of functional ionic liquids is comprehensively investigated. Moreover, some of them show obvious plastic crystal phase behaviors with rotational disorder and activated vacancies/defects, which can offer a solid bulk matrix for doping 1-propyl-3-methylimidazolium iodine (PMII), LiI an I_2 to prepare for plastic crystal electrolytes with high melting points and conductivity. Furthermore, the resulting solid-state dye-sensitized solar cell (DSSC) exhibits a power conversion efficiency (PCE) of 5.22% under the simulated air mass 1.5 solar spectrum illuminations at 100 mW cm^{-2}, and displays a superior long-term stability than conventional liquid-based devices. These results offer us a feasible method to explore new organic plastic crystals and electrolytes for high temperature solid-state DSSCs.

Introduction

Ionic liquids (ILs) are mostly liquid organic salts with melting points below/near room temperature.[1] During the last two decades, due to their negligible vapor pressure, high chemical and thermal stability and unique ionic environment, ionic liquids have been widely used as green and sustainable solvents for synthesis, catalysis and petrochemical industries.[2-3] In addition, high ionic conductivity, large viscosity range and wide electrochemical windows also render them as a promising source for liquid or solid electrolytes for renewable energy devices, such as lithium batteries and dye-sensitized solar cells.[4-5]

Recently, functional ionic liquids, with rationally designing structural groups, have attracted great attention for extended research interest. For example, rigidity and cubic structure of polyhedral oligomeric silsesquioxane (POSS) moiety can enhance the thermal stability and greatly reduce the melting temperature of the POSS ionic liquids.[6] By employing propylene carbonate, several polycarbonate (PC) functional ionic liquids are rationally designed with wide thermal stability and exhibit potential lithium metal deposition ability.[7] Ferrocene-based ionic liquids also represent excellent electroactive and fine charge transport properties, which extend the chemical diversity intrinsically redox ionic liquid phases.[8] In virtue of amine fixation function to form an ammonium carbamate, task-specific ionic liquids prove notable sequestration efficiency of CO_2.[9] Due to the formation of surface protective groups with lubricated metal surface by a tribochemical reaction and good miscibility of ILs with the polyurea grease, ILs also show a potential use as additives for the rolling bearings industry.[10] A variety of task specific ionic liquids (TSIL) can be used to prepare for N-doped microporous and mesoporous carbons with high surface area over 640 m^2 g^{-1}, highlighting exciting opportunities in functional carbon composites.[11] Full color-tunable luminescent emissions can be successfully achieved by simple tuning of changing moieties of the ionic liquid crystals, displaying potential applications in fluorescent sensors and optoelectronic materials.[12] Therefore, functional ionic liquids have offered an opening opportunity to demonstrate their basic research interest and promising extensive application.

Here, we design and synthesize a series of functional ionic liquids containing pyrrolidinium cations bearing alkyl nitrile moieties and anions (I^-, PF_6^- and $TFSI^-$). Their chemical structures and thermal properties are confirmed and charactered by Fourier transform infrared (FTIR) spectra, nuclear magnetic resonance (NMR) measurement, thermogravimetric (TGA) and differential scanning calorimetry (DSC) analyzers in detail, respectively. These ionic liquids exhibit different thermal properties, which are beneficial to understand the alkyl nitrile and anions structure effect. Notablely, some of synthesized ionic liquids represent obvious plastic crystal phases, which lead to high intrinsic ionic conductivity. As an application, doping an ionic liquid 1-propyl-3-methylimidazolium iodide (PMII) and LiI can still retain the plastic crystal behaviors, and further enhances the ionic conductivity of prepared high temperature solid state electrolytes without any volatile organic solvent for dye-sensitized solar cells (DSSCs). The fabricated DSSC shows high power conversion efficiency over 5%, and displays better long-term stability than that of referenced organic liquid electrolytes.

Experimental Procedure

Materials

Iodomethane, 1-pyrroleacetonitrile, 1-pyrrolidinepropanenitrile, 1-pyrrolidinobutyronitrile, lithium iodide (LiI), 4-*tert*-butylpyridine (TBP), 3-methoxypropionitrile (MPN) and iodine (I_2) were purchased

from Alfa Aesar and used as received. Potassium hexafluorophosphate (KPF_6), lithium bis(trifluoromethanesulfonyl)imide (LiTFSI), 1-propyl-3-methylimidazolium iodine (PMII) and 1,2-dimethyl-3-propylimidazolium iodide (DMPII) were purchased from Merck. H_2PtCl_6 and organic dye 2-Cyano-3-[5'''-(9-Ethyl-9H-carbazol-3-yl)-3',3'',3'''4-tetra-n-hexyl-[2,2',5',2'',5'',2'' ']-quaterthiophenyl -5-yl]acrylic acid (MK-2) were purchased from Aldrich. All the chemical reagents were used without further treatment. Fluorine-doped tin oxide (FTO) glass electrodes (8 Ω/Sq), and slurries containing 20 nm-sized mesoporous and 200 nm-diameter light-scattering TiO_2 colloidal were purchased from Dalian Hepat Chroma Solar Tech. Co., Ltd (China).

General synthesis procedure of 1-Cyanomethyl-1-methylpyrrolidinium iodide (CMMPI), 1-Cyanomethyl-1-methylpyrrolidinium hexafluorophosphate ($CMMPPF_6$) and 1-Cyanomethyl-1-methylpyrrolidinium bis(trifluoromethanesulfonyl)imide (CMMPTFSI):

CMMPI was synthesized as follows. Briefly, a mixture of iodomethane (20 mmol, 2.84 g) and 1-pyrrolidineacetonitrile (20 mmol, 2.2 g) in 20 mL ethanol was stirred at 60 °C for 12 h under an atmosphere of nitrogen. After the evaporation of solvent, the crude product was washed with diethyl ether three times, and dried under vacuum at 60 °C for 24 h to provide 4.59 g CMMPI (yield: 91%, brown powder). mp: 30.2 °C; ^{1}HNMR: (400 MHz, d_6-DMSO): 4.90 (s, 2H), 3.64-3.70 (m, 2H), 3.55-3.62 (m, 2H), 3.20 (s, 3H), 2.10-2.16 (m, 4H) (see ESI, Fig. S1).

Anion exchange of CMMPI with KPF_6 in aqueous solution yielded $CMMPPF_6$ (yield: 86%, brown powder). mp, 22.6 °C;^{1}HNMR: (400 MHz, d_6-DMSO): 3.69-3.75 (t, 2H), 3.42-3.58 (m, 4H), 3.17-3.24 (t, 3H), 3.02-3.07 (s, 3H), 2.05-2.15 (m, 4H) (see ESI, Fig. S1).

While, CMMPTFSI was synthesized by anion exchange of CMMPI with LiTFSI (yield: 85%, white powder). ^{1}HNMR: (400 MHz, d_6-DMSO): 4.86-4.90 (s, 2H), 3.64-3.72 (m, 2H), 3.20-3.24 (s, 3H), 2.12-2.20 (m, 4H) (see ESI, Fig. S1).

Synthesis of 1-Cyanoethyl-1-methylpyrrolidinium iodide (CEMPI), 1-Cyanoethyl-1-methylpyrrolidinium hexafluorophosphate ($CEMPPF_6$) and 1-Cyanoethyl-1-methylpyrrolidinium bis(trifluoromethanesulfonyl)imide (CEMPTFSI):

The same procedure was followed as described above, except for the use of 1-pyrrolidinepropionitrile (2.48 g, 20 mmol) instead of 1-pyrrolidineacetonitrile. CEMPI (yield: 88 %, brown powder); mp: 126 °C; ^{1}HNMR: (400 MHz, d_6-DMSO): 3.69-3.74 (t, 2H), 3.50-3.56 (m, 2H), 3.44-3.50 (m, 2H), 3.18-3.22 (t, 2H), 3.03 (s, 3H), 2.05-2.11 (m, 4H) (see ESI, Fig. S2). $CEMPPF_6$ (yield: 84 %, brown powder); mp,78 °C;^{1}HNMR: (400 MHz, d_6-DMSO): 3.68-3.75 (t, 2H), 3.44-3.58 (m, 4H), 3.17-3.24 (m, 2H), 3.03 (s, 3H), 2.04-2.16 (m, 4H) (see ESI, Fig. S2). CEMPTFSI (yield: 84 %, brown powder); ^{1}HNMR: (400 MHz, d6-DMSO): 3.69-3.75 (t, 2H), 3.42-3.58 (m, 4H), 3.17-3.24 (m, 2H), 3.04 (s, 3H), 2.06-2.14 (m, 4H) (see ESI, Fig. S2).

Synthesis of 1-Cyanopropyl-1-methylpyrrolidinium iodide (CPMPI), 1-Cyanopropyl-1-methylpyrrolidinium hexafluorophosphate ($CPMPPF_6$) and 1-Cyanopropyl-1-methylpyrrolidinium bis(trifluoromethanesulfonyl)imide (CEMPTFSI):

The same procedure was followed as described above, except for the use of 1-pyrrolidinobutyronitrile (2.74 g, 20 mmol) instead of 1-pyrrolidinepropionitrile. CPMPI (yield: 88 %, brown powder); mp: 141 °C; ^{1}HNMR: (400 MHz, d_6-DMSO): 3.44-3.57 (m, 4H), 3.36-3.42 (m, 2H), 3.02 (s, 3H), 2.61-2.67 (m, 2H), 2.03-2.13 (m, 6H) (see ESI, Fig. S3). $CPMPPF_6$ (yield: 84%, brown powder); mp, 226 °C; ^{1}HNMR: (400 MHz, d_6-DMSO): 3.40-3.56 (m, 4H), 3.35-3.40 (m, 2H), 3.0 (s, 3H), 2.58-2.65 (m, 2H), 2.02-2.15 (m, 6H) (see ESI, Fig. S3). CPMPTFSI (yield: 84 %, brown powder); ^{1}HNMR: (400 MHz, d_6-DMSO): 3.40-3.56 (m, 4H), 3.35-3.40 (m, 2H), 3.0 (s, 3H), 2.58-2.66 (m, 2H), 2.03-2.15 (m, 6H) (see ESI, Fig. S3).

Device fabrication

The fabrication of DSSCs was assembled as documented in the previous literature.[13] The cleaned FTO glass was covered at two parallel edges with an adhesive tape to control the thickness of mesoporous TiO_2 film. Two layers of TiO_2 particles were deposited onto cleaned FTO glass and used as photoelectrodes. A 10 μm thick film of 20 nm sized TiO_2 particles was deposited onto the FTO glass electrode by the doctor-blade technique. The film was dried at 125 °C for 5 min. Then, a second 5 μm thick layer of 200 nm light-scattering anatase particles were coated on the top of the first TiO_2 layer. The resulting TiO_2 films were annealed at 500 °C for 15 min. After cooling to 80 °C, the obtained TiO_2 electrode was immersed in 0.3 mM solution of MK-2 in anhydrous toluene at room temperature for 12 h. The dyed TiO_2 electrode was washed with anhydrous ethanol and dried with nitrogen stream. To prepare the Pt counter electrode, two drops of 5 mM H_2PtCl_6 in ethanol was placed onto the cleaned FTO glass substrate, followed by drying and annealing at 400 °C for 15 min.

The electrolytes A-G, composed of 0-40 wt% PMII and CPMPI with/without 0.1 M LiI and 0.10 M I_2, were heated at 120 °C and stirred for 8 h to ensure homogeneity. After cooling down to room temperature, all the solid-state electrolytes were formed.

DSSCs were fabricated by sandwiching the methanol solution of Electrolyte G between a dye-sensitized TiO_2 electrode and a pre-drilled Pt counter electrode by a 40 μm hot melt ring (Surlyn, DuPont). The resulting cells were placed in vacuum to remove air to guarantee optimum filling and fine electrical contact. The produced devices were sealed with a Surlyn sheet and a thin glass cover by heating.

Characterization and Measurements

^{1}HNMR spectra were recorded on a Varian 400 MHz spectrometer. Fourier transform infrared (FTIR) spectra of the synthesized compounds were recorded on a Varian CP-3800 spectrometer in the range of 4000–400 cm^{-1}. Thermal analysis was carried out on Universal Analysis 2000

thermogravimetric analyzer (TGA). Samples were heated from 50 to 500 °C at a heating rate of 10 °C min^{-1} under a nitrogen flow. Differential scanning calorimetry (DSC) measurements were performed under a nitrogen atmosphere with a heating rate of 10 °C min^{-1} in a temperature range of -50–300 °C on DSC-Q200. The conductivity of electrolytes was characterized in a cell composed of Teflon tube and two identical stainless steel electrodes on a CHI660c electrochemical workstation, using the AC impedance method over the frequency range 1-10^5 Hz. All the samples were equilibrated for at least 20 min at a given temperature. The photocurrent density-voltage (J-V) curves of the assembled DSSCs shielded by an aluminum foil mask with an aperture area of ≈0.25 cm^2 were measured with a digital source meter (Keithley, model 2400) under simulated air mass (AM) 1.5 solar spectrum illumination at 100 mW cm^{-2}. Incident photo-to-current conversion efficiency (IPCE) plotted as a function of excitation wavelength was recorded under the irradiation of a Xenon lamp with a monochromater (Oriel CornerstoneTM 260 1/4). The photoelectrochemical parameters, such as the fill factor (FF) and power conversion efficiency (PCE) were calculated according to the previous reports.[13]

Results and Discussion

Scheme 1 Synthetic procedures for the preparation of a series of functional ionic liquids containing pyrrolidinium cations bearing alkyl nitrile moieties.

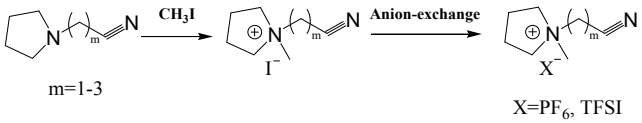

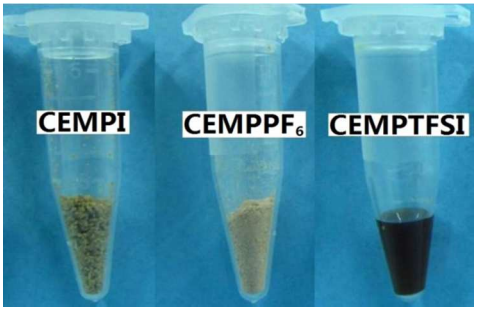

Fig. 1 Typical photographs of synthesized CEMPI, $CEMPPF_6$ and CEMPTFSI, respectively.

Scheme 1 shows the synthetic route and chemical structures of functional ionic liquids containing pyrrolidinium cations with different alkyl nitrile moieties and anions. The purity and chemical structure are confirmed by ^{1}HNMR (Fig. S1-3, ESI†) and FTIR spectrum. Meanwhile, Fig. 1 exhibits the typical photographs of CEMPI, $CEMPPF_6$ and CEMPTFSI. In addition, all of the photographs of synthesized compounds in this work can be found in Fig. S4. Obviously, compared with other compounds with anions of I^- and PF_6^-, CMMPTFSI, CEMPTFSI and CPMPTFSI display liquid state behavior, probably because of weaker van de Waals forces.[14]

As shown in Fig. 2, typically, the chemical structures of CPMPI, $CPMPPF_6$ and CPMPTFSI are confirmed by FTIR spectra. The bands attributed to the pyrrolidinium cations between 3300 and 3650 cm^{-1} are clearly identified. Morever, the adsorption peaks centred at 2900-3000 cm^{-1} and 1464 cm^{-1} are attributed to the C-H stretching vibration mode of the methylene chain and the alkyl chains. In all the FTIR spectrum, characteristic peaks of C≡N stretching vibrations at 2245 cm^{-1} are also observed. In addition, the anion exchange could be identified by the appearance of new bands. Compared with the absorption peak of anion I^- of CPMPI at 906 and 750 cm^{-1} in Fig. 1a, new bands corresponding to PF_6^- anion in Fig. 1b are observed at 841 and 560 cm^{-1}.[15] The characteristic absorption peaks at 1348, 1202 and 1055 cm^{-1} belonging to TFSI anion in Fig. 1c, are also highly intensified,[15,16] indicating the successful anion exchange. Meanwhile, all of the FTIR spectra of synthesized ionic liquids are shown in Fig. S5, revealing the similar results of anion exchange.

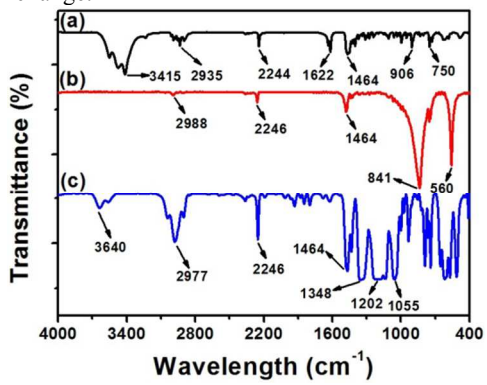

Fig. 2 FTIR spectra of (a) CPMPI, (b) $CPMPPF_6$ and (c) CPMPTFSI, respectively.

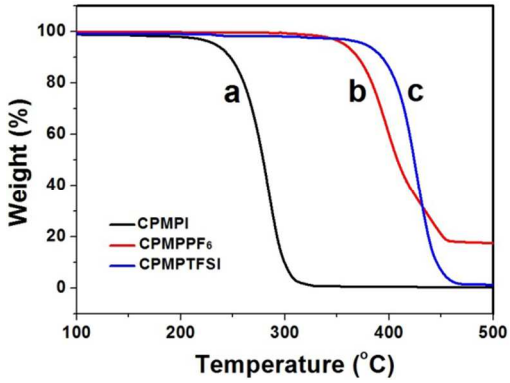

Fig. 3 TGA curves of (a) CPMPI, (b) $CPMPPF_6$ and (c) CPMPTFSI, respectively.

The influence of counteranions on the thermal stability of produced functional ionic liquids is studied as well. Fig. 3 shows the typical TGA curves of CPMPI, $CPMPPF_6$ and CPMPTFSI. The initial decomposition temperature of CPMPI is about 258 °C (Fig. 3a), indicating its high thermal stability. However, the anion exchange of CPMPI with PF_6^- and $TFSI^-$ represents much better thermostability, corresponding to values of 365 and 405 °C, respectively. The influence of anion structure on the thermal stability is in the order of $I^- < PF_6^- < TFSI^-$, in agreement with previous observation trends.[15] Meanwhile, the TGA curves of other ionic liquids with different alkyl nitrile moieties and anions

are shown in Fig.S6. The thermal properties of the ionic liquids are summarized in Table 1 as well. Corresponding values of CMMPI, $CMMPPF_6$ and CMMPTFSI are 204, 305 and 340 °C. Whereas, CEMPI, $CEMPPF_6$ and CEMPTFSI with methylene chain length of 2C represent much lower initial decomposition temperature (180, 212 and 202 °C) as previous reports,[17] probably for strong interaction of nitrile groups to pyrrolidinium rings. This result is also supported with the following DSC analysis.

Table 1 TGA and DSC results for functional ionic liquids.

	TGA	DSC			
	T_{onset} [a]	mp [b]	T_d [c]	$T_{S\text{-}S\ I}$ [d]	$T_{S\text{-}S\ II}$ [e]
CMMPI	204	30.2	209	14.1	-
$CMMPPF_6$	305	22.6	281	-	-
CMMPTFSI	340	-	-	-	-
CEMPI	180	126	187	-	-
$CEMPPF_6$	212	78	-	60	-
CEMPTFSI	202	-	-	-	-
CPMPI	258	141	285	121	95
$CPMPPF_6$	365	226	-	95	-
CPMPTFSI	405	-	-	-	-

[a] Initial decomposition temperature by TGA; [b] Melting point; [c] decomposition temperature by DSC on heating; [d] Temperature of solid-solid transition I; [e] Temperature of solid-solid transition II. [-] No measurement.

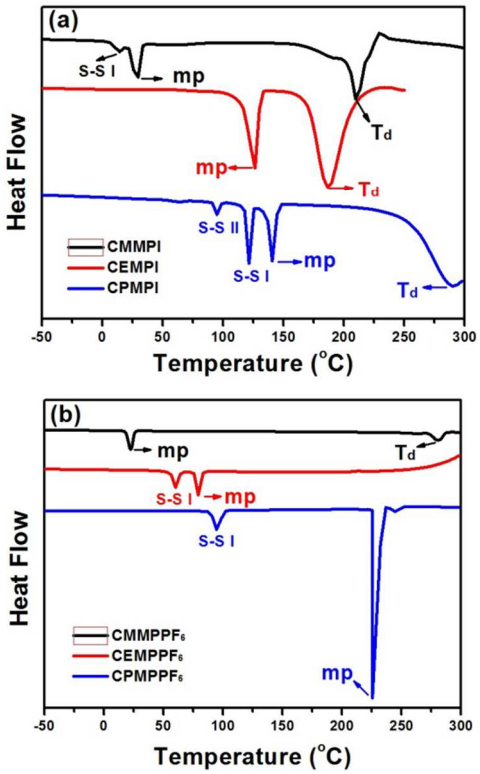

Fig. 4 The DSC curves of (a) CMMPI, CEMPI and CPMPI; (b) $CMMPPF_6$, $CEMPPF_6$ and $CPMPPF_6$, respectively.

Further investigation to thermal stability by differential scanning calorimetry (DSC) is shown in Fig. 4. The thermal properties of the ionic liquids are also summarized in Table 1. Obviously, the melting points generally increase along with increasing methylene chain length from 1C to 3C, because of high symmetry and low rotational degrees of freedom determined by enhanced van der Waals interactions.[18,19]. In Fig. 4a, the melting points of CMMPI, CEMPI and CPMPI are 30.2, 126 and 141 °C, respectively, whereas the decomposition temperatures (T_d) of them are 209, 187 and 285 °C. It should be pointed that methylene chain length with 2C significantly decreases the thermal stability of CEMPI, in accordance with the TGA result. As shown in Fig. 4b, the values of melting points increase in the order $CMMPPF_6$ < $CEMPPF_6$ < $CPMPPF_6$, corresponding to 30.2, 126 and 141 °C, respectively. More interestingly, CMMPI, CPMPI, $CEMPPF_6$ and $CPMPPF_6$ exhibit one or two solid-solid phase transition (S-S I and S-S II). The $T_{S\text{-}S\ I}$ values are 14.1, 60, 121 and 95 °C, respectively, suggesting wide plastic phase ranges. However, CPMPI also shows a solid-solid phase transition temperature at 95 °C, indicating another form of molecular rotamer. This unique phenomenon donates some ionic crystals as organic plastic crystals, which have been extensively investigated by MacFarlane's and other research groups.[18-24]

Organic plastic crystals are a kind of compounds composed of organic molecules which are rotationally disordered.[25] The existence of one or several solid-solid phase transitions below the melting point enables organic plastic crystals not only plastic properties and good mechanical flexibility, but also favorable rotational disorder and activated vacancies/defects, resulting in effective ions migration (Li^+, H^+, I^-, etc.) and high ionic conductivity. Therefore, solid state electrolytes based on organic plastic crystals have being widely used for lithium ion cells[20,26] and dye-sensitized solar cells,[27,28] representing great potential application in electrochemical devices.

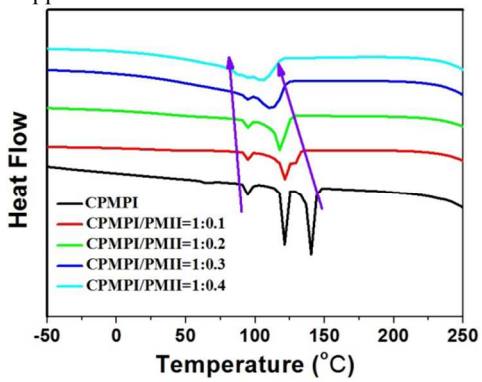

Fig. 5 DSC curves of CPMPI, and PMII doped CPMPI with different weight ratio, respectively.

Table 2 The components and conductivity of the electrolytes at room temperature in this work.

Electrolyte	PMII [wt%][a]	Conductivity [10^{-5} S/cm]	I_2 [M]	LiI [M]
Electrolyte A	0	4.23	-	-
Electrolyte B	10	6.15	-	-
Electrolyte C	20	7.73	-	-
Electrolyte D	30	9.08	-	-
Electrolyte E	40	10.12	-	-
Electrolyte F	40	37.43	0.1	-
Electrolyte G	40	42.58	0.1	0.1

[a] Weight ratios of PMII/CPMPI varies from 0 to 40 wt%.

The impressive plastic behaviors in synthesized compounds and discussion above trigger our interest in further exploring

the possibility to fabricate the solid state DSSCs based on the nitrile-functional plastic crystals. The relatively high melting point (141 °C) and solid-solid phase change temperatures (95 and 121 °C) render CPMPI as one of high temperature solid state electrolytes, which can overcome the leakage, evaporation and high temperature instability of conventional organic liquid electrolytes under practical outdoor conditions over 60-80 °C.[29] Therefore, as shown in Fig. 5, different weight ratio of PMII doped CPMPI based solid state electrolytes are prepared and characterized by DSC. Obviously, sequential addition of 10-40 wt% PMII greatly decreases the melting point of CPMPI. However, the solid-solid phase transition temperature ($T_{S\text{-}S\ I}$) just decreases from 121 to 107 °C, demonstrating that PMII doped CPMPI based solid state electrolytes still maintain solid state property and plastic behaviors. These results also indicate that PMII can be successfully incorporated into the bulk matrix of CPMPI to form a solid solution and act as effective ionic migration species for solid state electrolytes. It should be noted that 40 wt% PMII doped CPMPI plastic crystal electrolyte is completely solid at 100 °C, far beyond the outdoor operating requirement for solid state DSSCs.

It has been demonstrated that high ionic conductivity is critical to the performance of solid state DSSCs. Table 2 summarizes the conductivity for 0-40 wt% PMII doped CPMPI plastic crystal electrolytes with different I_2 and LiI contents (Electrolyte A-G). It can be clearly seen that the conductivity of all the solid state electrolytes increases with the PMII content. Compared with the pure CPMPI (4.23×10^{-5} S/cm) and other weight ratio of PMII doped Electrolyte A-D, 40 wt% PMII doped CPMPI Electrolyte E shows highest conductivity with the value of 1.01×10^{-4} S/cm, probably due to the high bulk conductivity of PMII (6.0×10^{-4} S/cm) and decoupling of rational disorder and the existence of vacancies and defects in the lattice of plastic crystal (CPMPI in this work).[21] Notablely, further doping I_2 into Electrolyte E can significantly enhance the conductivity of prepared Electrolyte F and G, respectively. This increase of ionic conductivity originates from the formation of polyiodides by the reaction of I^- and I_2 species,[30] accelerating the charge transport along the polyiodides chain by the Grotthus-type electron-exchange mechanism. The mechanism can also be expressed by the Dahm-Ruff equation (Equation 1).[31]

$$D_{app} = {}^1/_6\, k_{ex}\delta^2 c + D_{phys} \quad (1)$$

where D_{app} is apparent diffusion coefficient of I^- and I_3^-, D_{phys} is physical diffusion, k_{ex} is the rate constant of electron exchange, and c and δ are the concentration and average center-to-center distances between redox species, respectively. Thus, high conductivity of 3.74×10^{-4} S/cm for Electrolyte F is successfully obtained. In addition, introduction of LiI can be further incorporated into the matrix of Electrolyte F to form Electrolyte G, resulting in higher conductivity of 4.26×10^{-4} S/cm. Increased bulk concentration of iodide and Li^+ ions,[32] creation of vacancies and defects in the lattice of CPMPI as an additional charge carrier,[33] and the interaction between Li^+ and nitrile groups[34] facilitating the charge transfer of I^- along the ployiodides chain, should be responsible for the enhancement in conductivity of Electrolyte G. For these reasons, Electrolyte G is thereby chosen for the fabrication of solid-state DSSC in this work.

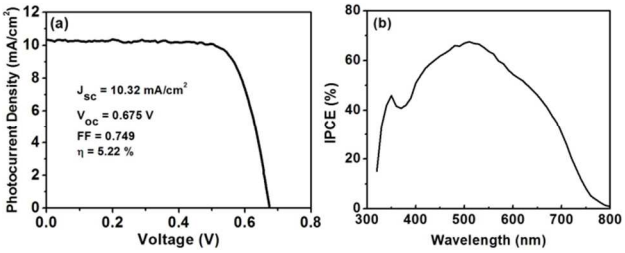

Fig. 6 a) Photocurrent density–voltage (*J–V*) curve and b) IPCE *vs.* wavelength profiles for the high temperature solid-state DSSC based on Electrolyte G. Cell area: 0.25 cm^2.

Photocurrent density–voltage (*J–V*) curve of the fabricated device based on Electrolyte G is shown in Fig. 6a. The values of open-circuit voltage (V_{oc}), short-circuit current density (J_{sc}), fill factor (FF) are 0.675 V, 10.32 mA/cm^2 and 0.749, respectively, yielding a power conversion efficiency (PCE) of 5.22%. Meanwhile, as shown in Fig. 6b, the incident photon-to-current conversion efficiency (IPCE) exceeds 50% in a broad spectral range from 400 to 650 nm, and reaches the maximum value of about 67.5% at 510 nm, indicating high light harvesting efficiency, fast electron injection, effective dye regeneration and charge collection for the high temperature solid-state DSSC.

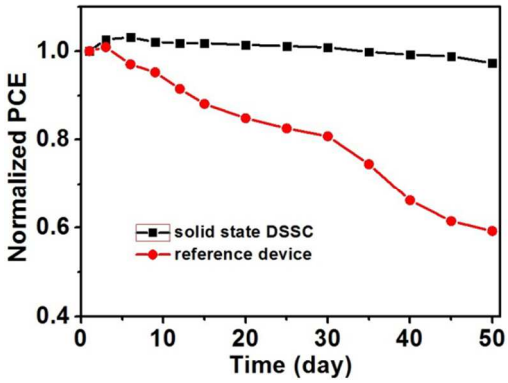

Fig. 7 Time-course variation of normalized PCE for fabricated solid-state DSSC and reference device with successive one sun light soaking during accelerated aging test at 60 °C, respectively. A typical organic liquid electrolyte for reference device contains 0.6 M DMPII, 0.1 M LiI, 0.5 M TBP, 0.1 M I_2 in MPN.[13]

The long-term stabilities of the solid-state DSSC above and reference device containing an organic liquid electrolyte at 60 °C under the same condition are also investigated and presented in Fig. 7. During the first three days, the efficiency is moderately enhanced along with an increase of J_{sc} origining from the regeneration of dye MK-2 and improvement of the interfacial contact between TiO_2 and the plastic crystal electrolyte.[35,36] More importantly, due to the high temperature solid property of the employed plastic electrolyte, the solid-state DSSC still remains almost over 97% of its initial conversion efficiency after the 50 days' aging test, representing excellent stability. For comparison, reference device fabricated with an organic liquid electrolyte just

maintains about 60% of its initial conversion efficiency. These results of the stability tests demonstrate that fabricated solid-state DSSC could overcome the leakage and evaporation of organic components in conventional DSSCs.

Conclusions

In summary, a series of functional ionic liquids based on pyrrolidinium cations bearing alkyl nitrile moieties have been designed, synthesized and charactered. They are successfully prepared with high purity and yield. With respect to the anion structure, the thermal stability is in the order of I^- < PF_6^- < $TFSI^-$. Meanwhile, increasing the methylene chain length from 1C to 3C of pyrrolidinium cations bearing alkyl nitrile moieties can increase the melting points of the solid ionic crystals. Moreover, some of them show obvious plastic crystal phase behaviors with rotational disorder and activated vacancies/defects, which can offer a solid bulk matrix for doping PMII, LiI an I_2 to prepare for plastic crystal electrolytes with high conductivity. Furthermore, the fabricated high temperature solid-state DSSC exhibits a high efficiency of 5.22%, and displays more excellent long-term stability than conventional liquid-based devices. These results offer us a feasible method to organic plastic crystals and electrolytes for high performance solid-state DSSCs in future practical applications.

Acknowledgements

This work was supported by Postdoctoral Science Foundation Grant of China (No. 2013M531397), University Science Research Project of Jiangsu Province (No. 13KJB150033), the Natural Science Foundation of Jiangsu Province (No. BK20140311), the Open Foundation of Jiangsu Key Laboratory of Thin Films and the Project Funded by the PAPD of Jiangsu Higher Education Institutions.

Notes and References

[a] *College of Physics, Optoelectronics and Energy & Collaborative Innovation Center of Suzhou Nano Science and Technology, Soochow University, Suzhou215006, P.R.China. Fax: +86-512-65228130; Tel: +86-512-65228130; E-mail: jzhao@suda.edu.cn; zouguifu@suda.edu.cn*
[b] *Jiangsu Key Lab of Thin Films, Soochow University.*
Electronic Supplementary Information (ESI) available: Additional tables (PDF). See DOI: 10.1039/b000000x/

1 R. D. Rogers, K. R. Seddon and S. Volkov, *In Green Industrial Applications of Ionic Liquids*; NATO Science. Series; Kluwer: Boston, 2002.
2 T. Welton, *Chem. Rev*., 1999, **99**, 2071-2083.
3 V. I. Pârvulescu and C. Hardacre, *Chem. Rev*., 2007, **107**, 2615-2665.
4 M.Armand, K. Endres, D. R. MacFarlane, H. Ohno and B. Scrosati, *Nat. Mater*., 2009, **8**, 621-629.
5 S. M. Zakeeruddin, and M. Grätzel, *Adv. Funct. Mater*., 2009, **19**, 2187-2202.
6 K. Tanaka, F. Ishiguro and Y. Chujo, *J. Am. Chem. Soc.,* 2010, **132**, 17649-17651.
7 T. Tsuda, K. Kondo, T. Tomioka, Y. Takahashi, H. Matsumoto, S. Kuwabata and C. L. Hussey, *Angew. Chem. Int. Ed*., 2010, **50**, 1310-1313.
8 R. Balasubramanian, W. Wang and R. W. Murray, *J. Am. Chem. Soc*., 2006, **128**, 9994-9995.
9 E. D. Bates, R. D. Mayton, I. Ntai and Jr. J. H. Davis, *J. Am. Chem. Soc*., 2002, **124**, 926-927.
10 M. Cai, Z. Zhao, Y. Liang, F. Zhou and W. Liu, *Tribol. Lett.,* 2010, **40**, 215-224.
11 J. S. Lee, Q. Wang, H. Luo, G. A. Baker and S. Dai, *J. Am. Chem. Soc*., 2009, **131**, 4596-4597.
12 K. Tanabe, Y. Suzui, M. Hasegawa and T. Kato, *J. Am. Chem. Soc., 2012*, **134**, 5652-5661.
13 J. Zhao, F. Yan, L. Qiu, Y. Zhang, C. Chen, B. Sun, *Chem. Commun*., 2011, **47**, 11516-11518.
14 N. V. Plechkova and K. R. Seddon, *Chem. Soc. Rev*., 2008, **37**, 123-134.
15 J. Zhao, F. Yan, Z. Chen, H. Diao, F. Chu, S. Yu and J. Lu, *J. Polym. Sci., Part A: Polym. Chem*, 2009, **47**, 746–753.
16 X. Chen, J. Zhao, J. Zhang, L. Qiu, D. Xu, H. Zhang, X. Hang, B. Sun, G. Fu, Ye, Zhang, F. Yan. *J. Mater. Chem*., 2012, **22**, 18018-18024.
17 S. Schneider, T. Hawkins, Y. Ahmed, S. Deplazes, J. Mills. "*Ionic Liquid Fuels for Chemical Propulsion*" *ACS Symp. Ser*. 2012, **111**(*In Ionic Liquids: Science and Application*), 1-25.
18 S. J. Pas, J. M. Pringle, M. Forsyth, D. R. MacFarlane, *Phys. Chem. Chem. Phys*., 2004, **6**, 3721-3725.
19 Z. Zhou, H. Matsumoto, K. Tatsumi, *ChemPhysChem* 2005, **6**, 1324-1332.
20 D. R. MacFarlane, J. Huang, M. Forsyth, *Nature* 1999, **402**, 792-794.
21 D. R. MacFarlane, M. Forsyth, *Adv. Mater*., 2001, **13**, 957-966.
22 J. M. Pringle, P. C. Howlett, D. R. MacFarlane, M. Forsyth, *J. Mater. Chem*., 2010, **20**, 2056-2062.
23 Y. Abu-Lebdeh, P. J. Alarco, M. Armand. *Angew. Chem. Int. Ed*., 2003, **42**, 4499-4501.
24 Z. Zhou, H. Matsumoto, K. Tatsumi, *ChemPhysChem* 2004, **10**, 6581-6591.
25 J. Adebahr, A. J. Seeber, D. R. MacFarlance, M. Forsyth, *J. Phys. Chem B*, 2005, **109**, 20087-20092.
26 P. J. Alarco, Y. Abu-Lebdeh, A. Abouimrane, M. Armand, *Nat. Mater*., 2004, **3**, 476-481.
27 V. Armel, M. Forsyth, D. R. MacFarlane, J. M. Pringle, *Energy Environ. Sci*., 2011, **4**, 2234-2239.
28 Q. Li, J. Zhao, B. Sun, B. Lin, L. Qiu, Y. Zhang, X. Chen, J. Lu, F. Yan, *Adv. Mater*., 2012, **24**, 945-950.
29 M. Grätzel, *J. Photochem. Photobiol A*, 2004, 164, 3-14.
30 J. H. Wu, S. C. Hao, Z. Lan, J. M. Lin, M. L. Huang, Y. F. Huang, P. J. Li, S. Yin, T. Sato, *J. Am. Chem. Soc*., 2008, **130**, 11568-11569.
31 R. Kawano, M. Watanable, *Chem. Commun*., 2005, 2107-2109.
32 Q. Li, X. Chen, J. Zhao, L. Qiu, Y. Zhang, B. Sun, F. Yan, *J. Mater. Chem*., 2012, **22**, 6674-6679.
33 Y. Shekibi, J. M. Pringle, J. Sun, S. J. Pas, N. M. Rocher, B. R. Clare, A. J. Hill, D. R. Macfarlane, M. Forsyth, J. *Mater. Chem*., 2010, **20**, 338-344.
34 H. X. Wang, B. F. Xue, Y. S. Hu, Z. X. Wang, Q. B. Meng, X. J. Huang, L. Q. Chen, *Electrochem. Solid-State Let*., 2004, **7**, A302-A305.
35 B. A. Gregg, F. Pichot, S. Ferrere and C. L. Fields, *J. Phys. Chem. B*, 2001, **105**, 1422–1429.
36 H. Wang, J. Li, F. Gao, G. Zhou and Z. Wang, *J. Am. Chem. Soc*., 2013, **135**, 12627-12633.